IET Communications

Research Article

IET Journals
The Institution of Engineering and Technology

NOMA-based cooperative relaying for secondary transmission in cognitive radio networks

ISSN 1751-8628
Received on 29th October 2018
Revised 5th April 2019
Accepted on 25th April 2019
E-First on 11th June 2019
doi: 10.1049/iet-com.2018.6075
www.ietdl.org

Yuzhi Chu[1,2] ✉, Benoit Champagne[3], Wei-Ping Zhu[4]

[1]*Department of Computer Sciences and Technology, Nanjing Tech. University, 30 Puzhunan Road, Nanjing, People's Republic of China*
[2]*Key Lab of Broadband Wireless Communication and Sensor Network Technology, Nanjing University of Posts and Telecommunications, Ministry of Education, Nanjing, People's Republic of China*
[3]*Department of Electrical and Computer Engineering, McGill University, Montreal, QC, Canada*
[4]*Department of Electrical and Computer Engineering, Concordia University, Montreal, QC, Canada*
✉ *E-mail: yuzhi_chu@163.com*

Abstract: In this study, the authors present and investigate a novel cooperative relaying scheme for cognitive radio networks (CRNs), which is based on non-orthogonal multiple access (NOMA). In the proposed scheme, following the detection of an idle channel, the secondary base station transmits a power domain NOMA signal to a first nearby secondary user (SU). In addition to decoding its own signal, this user applies a decode-and-forward strategy to relay the signal intended to a second SU. In contrast to previous works, where the spectrum sensing and transmission phases are treated separately, the authors here consider both phases jointly in the design and analysis of the proposed scheme. To characterise performance of the latter, analytical expressions are derived for the outage probability and the ergodic rate of the two SUs by assuming a flat Rayleigh fading channel model. The performance of two traditional orthogonal multiple access schemes is also analysed for comparison. Simulation and numerical results are presented to demonstrate the effectiveness of the proposed cooperative relaying scheme for CRN, as well as the accuracy of the analytical results.

1 Introduction

1.1 Related works

Non-orthogonal multiple access (NOMA) is considered as a key multiple access technology for fifth generation (5G) wireless networks. Compared to traditional orthogonal multiple access (OMA), NOMA offers significant advantages, including enhanced spectrum efficiency and network capacity [1–4]. The distinguishing feature of NOMA is to allow multiple users to share the same time-frequency resources via power-domain multiple access, sparse code multiple access or pattern division multiple access. In power-domain NOMA, users with better radio channels are allocated less power, which allows a flexible tradeoff between system performance and user fairness. The receivers with better channels implement successive interference cancellation (SIC), whereby they first decode the signals intended for users with poorer channels, and then remove these signals before decoding their own. The receivers with poorer channel conditions do not perform SIC and simply treat the signals of other users as noise.

Cooperative communication has attracted great attention as a means to increase diversity and extend network coverage. The study of NOMA within the cooperative framework was considered in [5–11], where advanced relaying techniques have been used to assist users suffering from weak channel conditions. The performance of NOMA-based downlink amplify-and-forward relaying over Nakagami-*m* fading channels was analysed in [5]. A full-duplex (FD) device-to-device-aided cooperative NOMA scheme was analysed in [6]. The performance of NOMA-based FD relaying was analysed and optimised in [7]. The power allocation problem for both half-duplex (HD) and FD cooperative NOMA systems was investigated in [8], with the aim to maximise the minimum achievable rate for a NOMA user pair. The performance of FD and HD relaying with cooperative NOMA was analysed in [9, 10] where it was shown that FD relaying can achieve a better performance than its HD counterpart in the low signal-to-noise ratio (SNR) regime. An optimal power allocation and multi-mobile users scheduling for NOMA relay-transmission was investigated in [11] to increase the throughput gain of the NOMA relay. Numerical results from the aforementioned studies generally show that cooperative NOMA can yield better outage performance and throughput than OMA.

Meanwhile, another means to improve spectrum efficiency is that of cognitive radio networks (CRNs) [12–14], which allows secondary users (SUs) to coexist with primary users (PUs) in the same frequency band as long as the SUs meet certain constraints to protect PUs. Within this context, cooperation among distributed nodes may further improve diversity and increase system performance for both PUs and SUs [15–18]. Ganesan and Li [15] illustrated the benefits of cooperative spectrum sensing in CRN, by showing that it can lead to an improved detection performance in a simple two-user network. A cooperative spectrum sensing scheme for multiuser single carrier networks without centralised control was proposed in [16]. The optimal power allocation and beamforming scheme minimising the outage probability of SUs with relay was derived in [17]. Elmahdy *et al.* [18] studied cooperative CRN with the objective of optimising the QoS for the SU while sustaining a target QoS for the PU.

Based on the aforementioned studies, it can be concluded that cooperative CRN can enhance spectrum efficiency through improved spectrum sensing, interference mitigation and transmission [19, 20]. Within this exacting framework, the consideration of NOMA provides a new and promising research avenue to further improve the spectral efficiency and system performance of both PUs and SUs [21–26]. NOMA was applied to a large-scale underlay CRN with randomly deployed users in [21], where the secondary base station (SBS) must satisfy a predefined power constraint to avoid interference at the PUs. A NOMA-based cooperative transmission scheme was proposed for a particular CRN scheme in [22], where the best SU acts as a relay to forward the PU's and SUs' messages. Based on available channel state information (CSI), [23] proposed three different SU scheduling strategies for cooperative NOMA in CRN. A novel NOMA-based cooperative transmission scheme was proposed in [24], where the SUs adopt NOMA to relay the primary signal and transmit SUs' data simultaneously. A cooperative NOMA scheme is investigated in [25] for an underlay CRN, where a SU with better channel gain

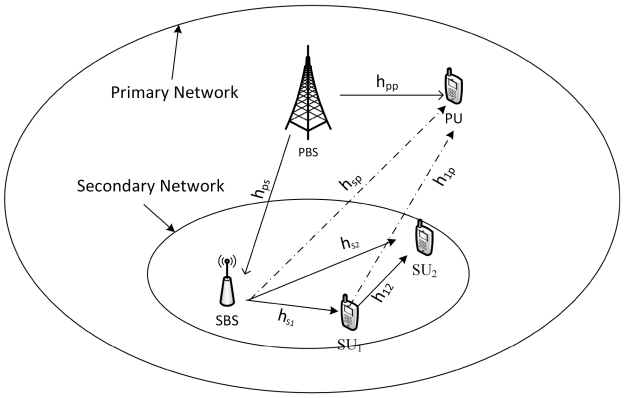

Fig. 1 *Downlink CRN system model comprising a primary and a secondary network*

is properly selected as a relay for assisting another SU with poor channel gain in the presence of a primary network. Mohammadi *et al.* [26] considered a NOMA-based CRN model, where a FD multi-antenna relay assists transmission from an access point (AP) to a distant SU, while the AP simultaneously transmits to a nearby SU. These studies and numerical results show that the consideration of NOMA within the cooperative CRN framework can significantly improve the performance of both primary and secondary networks.

1.2 Motivations and contributions

In particular, existing research on the incorporation of NOMA in the cooperative CRN framwork has shown the possibility to meet some of the more stringent 5G requirements in terms of high spectrum efficiency, increased base station capacity and improved QoS [27]. In spite of these potential benefits, implementing an efficient NOMA-based cooperative relaying scheme in CRN remains challenging in practice, because both NOMA and CRN are interference-limited. Specifically, the coexistence of the inter-network interference between primary and secondary networks and the intra-network interference caused by NOMA will result in a transmission performance degradation. Therefore, it is necessary to combine NOMA with CRN in an appropriate manner to limit inter-user interference at the PU and better utilise the underlying spectrum resources.

While in the above studies, NOMA was mainly used to improve the spectrum utilisation for the PU in the data transmission phase [21–26]. However, as discussed in [28], a cognitive transmission process contains two phases, namely: spectrum sensing and data transmission. Conceptually, these two phases cannot be designed and analysed separately, since they affect each other. For example, increasing the spectrum sensing time improves the detection performance, so that the PU can be better protected. However, from the SUs' perspective, this leads to a reduction of the data transmission time, thereby reducing spectral efficiency. Zhang *et al.* [29] have investigated the power control and sensing time optimisation problem in a cognitive small cell network, and [30] addressed the optimisation of sensing time and power allocation in CRN. While these works examined the interaction between energy efficiency and throughput, they did not consider the use of NOMA for improving transmission performance in cooperative CRN.

In this paper, we jointly consider the spectrum sensing and data transmission phases and propose a novel NOMA-based *relaying* strategy for CRN. The proposed scheme fills the gap between the traditional underlay and interweave CRN models [31, 32], in the sense that both PU and SU devices are allowed to simultaneously transmit over the same band, while spectrum sensing is employed to constrain the transmission power of the SUs. We then derive new analytical expressions for the outage probability and ergodic sum rate of the SUs, and finally examine the impact of the time allocation between spectrum sensing and data transmission on the overall system performance. Our main contributions are summarised as follows:

- We propose a NOMA-based cooperative transmission scheme to achieve better utilisation of the spectrum, where a nearby SU can act as a decode-and-forward (DF) relay to a distant SU. The proposed scheme allows the SUs, whose signals are superimposed in the power domain using NOMA, to access the licensed band for the whole duration of the data transmission phase. In addition, to limit interference to the PU, the transmission power of the SUs is constrained based on the result of the spectrum sensing phase.
- We derive new analytical expressions for the SUs' outage probability and the ergodic sum rate in order to examine the impact of the spectrum sensing time on these performance metrics. For performance comparison, we also analyse two existing traditional OMA-based schemes and obtain closed-form expressions for their outage probabilities and ergodic sum rates.
- Finally, numerical results are presented to demonstrate the effectiveness of the proposed scheme and the accuracy of the analytical results. Compared with OMA-based schemes, the system performance of our NOMA scheme in terms of the average outage probability is improved especially when the distant SU suffers from poor channel conditions.

1.3 Organisation and notation

This paper is organised as follows. In Section 2, the system model and the proposed NOMA-based cooperative transmission scheme are introduced. Section 3 investigates the outage probability of the proposed NOMA scheme and that of two traditional OMA schemes. Section 4 subsequently investigates the ergodic sum rate of these three schemes. Numerical and simulation results are presented in Section 5. Finally, Section 6 concludes the paper.

The following notations are employed in the paper: $Q(\cdot)$ is the complementary distribution function of the standard Gaussian, i.e. $Q(x) = (1/\sqrt{2\pi})\int_x^\infty \exp(-(t^2/2))\mathrm{d}t$; $\mathbb{E}[\cdot]$ denotes the expectation operation; $\mathcal{CN}(0, \sigma^2)$ denotes a complex Gaussian random variable with mean zero and variance σ^2; $f_X(\cdot)$ and $F_X(\cdot)$ denote the probability density function (PDF) and cumulative distribution function of a random variable X.

2 Proposed NOMA-based cooperative transmission scheme for CRN

2.1 System model

As shown in Fig. 1, we consider a downlink CRN system model featuring a primary network and a secondary network. The former includes a primary base station (PBS) and a primary user (PU), while the latter includes a NOMA-based SBS and two SUs (SU_1 and SU_2). Seven wireless links are involved in this model, namely: PBS-PU, PBS-SBS, SBS-PU, SBS-SU_1, SBS-SU_2, SU_1-SU_2 and SU_1-PU whose channel responses are represented by h_{pp}, h_{ps}, h_{sp}, h_{s1}, h_{s2}, h_{12} and h_{1p}, respectively.

In the proposed scheme, the use of NOMA allows the SBS to simultaneously transmit the two SUs' signals on the same band, thereby enhancing spectral utilisation. Specifically, SBS first detects an unoccupied licensed channel, and then uses this channel for its data transmission to SU_1 and SU_2 under an interference power constraint at the PU. However, due to the existence of interference and heterogeneity of the wireless channels, there is an imbalance between the reception quality of the two SUs. Assuming without loss of generality that SU_1 benefits from a better channel than SU_2, the former acts as a DF relay. That is, SU_1 takes advantage of SIC to first decode the signal intended to SU_2 and forward it to the latter, then SU_1 cancels the SU_2's signal to acquire its own signal.

The complete secondary transmission process is divided into two phases: spectrum sensing of the licensed band followed by data transmission from SBS to SU_1 and SU_2 based on NOMA. The time allocation between the two phases is depicted in Fig. 2*a*, where the spectrum sensing and the transmission phases, respectively, occupy a fraction τ and $1-\tau$ of the available time slot duration T (where $0 < \tau < 1$). Furthermore, the data transmission

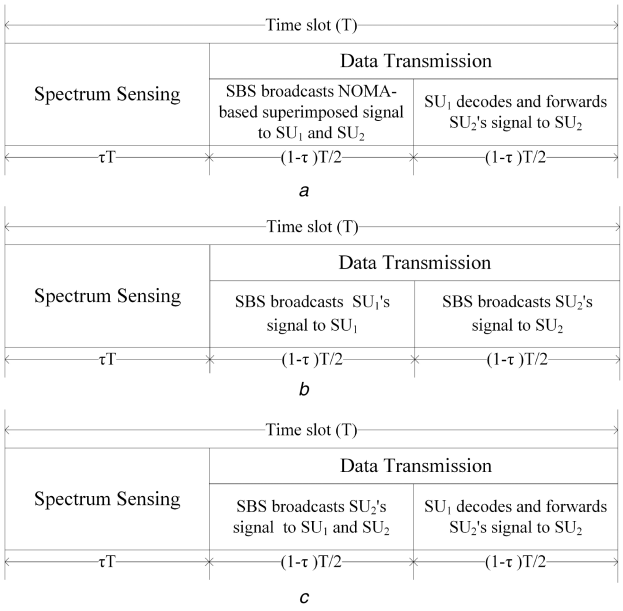

Fig. 2 *Allocation of time between the spectrum sensing and data transmission phases*
(a) NOMA-based scheme, ***(b)*** OMA-I scheme, ***(c)*** OMA-II scheme

phase is subdivided into two equal parts, i.e. broadcasting from SBS followed by relaying by SU_1. Throughout the paper, we make the following assumptions:

1. All devices or nodes in the network are equipped with a single antenna and work in HD mode, i.e. the same antenna can be used for either transmission or reception. In order to make our approach more valuable in practical applications, we will discuss the possible extension of our work to multiple antennas SBS in Section 5.3.
2. We consider narrowband transmission with flat fading channel between any two nodes. The corresponding channel coefficients, i.e. h_i where $i \in \{\text{pp}, \text{ps}, \text{sp}, \text{s1}, \text{s2}, 12, 1\text{p}\}$, are modelled as mutually independent complex random variables with Rayleigh fading distribution. That is, the PDF of their squared magnitude is given by $f_{|h_i|^2}(x) = (1/\sigma_i^2)\exp(-(x/\sigma_i^2))$ where $x \geq 0$ and σ_i^2 is the variance.
3. We assume that the channel condition of the SBS-SU_1 link is better than that of the SBS-SU_2 link, i.e. $\sigma_{s1}^2 \geq \sigma_{s2}^2$. This occurs for instance when SU_2 is located close to the edge of the secondary network.
4. We assume that the secondary network is located close to the edge of the primary network, and that the power level of the received signal from the PBS at SU_1 or SU_2 is much lower than that of the received signal from the SBS, so that the PBS signal component can be neglected in the analysis (see also [21, 23]).
5. We assume perfect CSI and SIC in this paper to simplify the mathematical analysis, which is a common approach used in many other published works in this area (e.g. [5, 7, 8]). Although we have assumed that the transmitter nodes know the perfect CSI of the channels and perfect subtraction of interfering user signals is performed with no residual interference incurred, the results of the proposed scheme will serve as useful theoretical bounds for practical channels. In order to make our approach more valuable in practical applications, the effects of imperfect CSI and that of imperfect SIC will be later discussed in Section 5.1 and 5.2, respectively.

2.2 Proposed NOMA-based transmission scheme

Below, we provide further explanations about the spectrum sensing and data transmission phases of the proposed scheme. We also derive preliminary results on detection performance and transmission power levels, which will be needed in our subsequent analysis.

2.2.1 Spectrum sensing phase.: During the spectrum sensing phase, the SBS first monitors a given spectral band which is potentially used by the PBS. Let H_μ for $\mu \in \{0, 1\}$ represent the PBS's state, where hypothesis H_0 (H_1) means that the licensed channel is unoccupied (occupied) by the PBS. Similarly, the result of spectrum sensing, i.e. signal detection at the SBS, is denoted by $\widehat{H}_\nu$ for $\nu \in \{0, 1\}$, where $\widehat{H}_0$ ($\widehat{H}_1$) indicates that a spectrum hole is available (not available).

Conditioned on the PBS state, the received signal at SBS can be expressed as

$$y(n) = \begin{cases} n_s(n), \\ \sqrt{P_p} h_{\text{ps}} x_p(n) + n_s(n), \end{cases} \tag{1}$$

where $n \in \{0, 1, \ldots, N-1\}$ is the discrete-time index, $N = \tau T f_s$ is the total number of available sensing samples and f_s is the sampling frequency[30]. Denoting by W the width of the licensed band under test, the sampling frequency can be chosen as $f_s = 2W$. In addition, $n_s(n)$ is a circular complex Gaussian white noise with mean zero and variance $E\{|n_s(n)|^2\} = P_n$, P_p is the transmission power of the PBS and $x_p(n)$ is the (normalised) signal broadcasted by the PBS with mean zero and unit variance, i.e. $E\{|x_p(n)|^2\} = 1$.

In this work, we adopt an energy detector for purpose of analysing the spectrum sensing performance; hence, the test statistic is given by

$$T(y) = \frac{1}{N} \sum_{n=0}^{N-1} |\, y(n) \,|^2 \ . \tag{2}$$

According to the central limit theorem, for a large N, the test statistic $T(y)$ under H_0 can be approximated by a Gaussian distribution with mean $\mu_0 = P_n$ and variance $\sigma_0^2 = P_n^2/N$ (see [30]). Denoting the detection threshold by θ, the probability of false alarm is given by

$$P_f = \Pr(T(y) > \theta | H_0) = Q\Big(\Big(\frac{\theta}{P_n} - 1\Big)\sqrt{N}\Big). \tag{3}$$

Similarly, under H_1, the test statistic $T(y)$ can be approximated by a Gaussian distribution with mean $\mu_1 = P_p\sigma_{\text{ps}}^2 + P_n$ and variance $\sigma_1^2 = (1/N)\big(5P_p^2\sigma_{\text{ps}}^4 + P_n^2\big)$. Thus, the probability of detection (i.e. $\Pr(T(y) > \theta | H_1)$) can be written as

$$P_d = Q\Big(\Big(\frac{\theta}{P_n} - \rho_p\sigma_{\text{ps}}^2 - 1\Big)\sqrt{\frac{N}{5\rho_p^2\sigma_{\text{ps}}^4 + 1}}\Big), \tag{4}$$

where we define the power ratio $\rho_p = \frac{P_p}{P_n}$. For a target probability of false alarm P_f, we can obtain that

$$\theta = P_n\Big(\frac{Q^{-1}(P_f) + \sqrt{N}}{\sqrt{N}}\Big), \tag{5}$$

$$P_d = Q\Big(\big(Q^{-1}(P_f) - \sqrt{N}\rho_p\sigma_{\text{ps}}^2\big)\frac{1}{\sqrt{5\rho_p^2\sigma_{\text{ps}}^4 + 1}}\Big). \tag{6}$$

In practice, the PBS alternates between the *on* and *off* states. A Bernoulli distribution with parameters p and q is used to model the PBS's state, where p and q are the probabilities that the licensed channel be on and off, respectively, with $0 < p < 1$ and $p + q = 1$. Let $\phi_{\mu\nu} = \Pr(H_\mu, \widehat{H}_\nu)$, for $\mu, \nu \in \{0, 1\}$, denote the probability of the different spectrum sensing events. We can write

$$\begin{cases} \phi_{00} = q(1 - P_f), & \phi_{01} = qP_f, \\ \phi_{10} = p(1 - P_d), & \phi_{11} = pP_d, \end{cases} \tag{7}$$

while the probability of SBS's spectrum sensing result $\widehat{H}_\nu$ is given by

$$\begin{cases}\Pr(\widehat{H}_0) = \phi_{00} + \phi_{10} = 1 - qP_f - pP_d, \\ \Pr(\widehat{H}_1) = \phi_{01} + \phi_{11} = qP_f + pP_d\,. \end{cases} \tag{8}$$

2.2.2 Data transmission phase.: As shown in Fig. 2*a*, during the first half of the transmission interval, the SBS broadcasts the superimposed NOMA signal to SU_1 and SU_2. The NOMA signal $x_s(n)$ can be written as

$$x_s(n) = \sqrt{P_{s|\nu}}(\sqrt{\alpha_1}x_1(n) + \sqrt{\alpha_2}x_2(n)), \tag{9}$$

where $P_{s|\nu}$ is the transmission power of the SBS under spectrum sensing result $\widehat{H}_\nu$, $x_1(n)$ and $x_2(n)$ are the (statistically independent) signals intended for SU_1 and SU_2 each with zero mean and unit variance, respectively, while $\alpha_1 > 0$ and $\alpha_2 > 0$ denote the power allocation coefficients for SU_1 and SU_2 with $\alpha_1 + \alpha_2 = 1$. In addition, $\alpha_1 \le \alpha_2$ since the SBS-SU_1 channel is better than the SBS-SU_2 one. Then, the received signals at SU_1, SU_2 and PU are given by

$$y_{1,1}(n) = h_{s1}x_s(n) + n_{s1}(n), \tag{10}$$

$$y_{2,1}(n) = h_{s2}x_s(n) + n_{s2}(n), \tag{11}$$

$$y_{p,1}(n) = h_{sp}x_s(n) + \sqrt{P_p}h_{pp}\mu x_p(n) + n_p(n), \tag{12}$$

where $n_{s1}(n)$, $n_{s2}(n)$ and $n_p(n)$ are statistically independent circular complex Gaussian noise terms with mean zero and variance P_n.

According to the SIC principle, SU_1 first decodes $x_2(n)$ by treating $x_1(n)$ as noise, and cancels it to acquire $x_1(n)$. In addition, our analysis of NOMA transmission is based on the ideal assumption of perfect subtraction of previous user signals in SIC with no residual interference incurred (see also [7, 8]). Based on (10), the effective received signal-to-interference-plus-noise ratios (SINR) of $x_2(n)$ and $x_1(n)$ at SU_1 are, respectively, given by

$$\gamma_{1,2|\nu} = \frac{\alpha_2 \mid h_{s1} \mid^2}{\alpha_1 \mid h_{s1} \mid^2 + \frac{1}{\rho_{s|\nu}}}, \tag{13}$$

$$\gamma_{1,1|\nu} = \alpha_1 \mid h_{s1} \mid^2 \rho_{s|\nu}, \tag{14}$$

where we define $\rho_{s|\nu} = P_{s|\nu}/P_n$. Similarly, based on (11), the received SINR of $x_2(n)$ at SU_2 is given by

$$\gamma_{2,2|\nu} = \frac{\alpha_2 \mid h_{s2} \mid^2}{\alpha_1 \mid h_{s2} \mid^2 + \frac{1}{\rho_{s|\nu}}}. \tag{15}$$

Let $\hat{x}_1(n)$ and $\hat{x}_2(n)$, respectively, denote the decoded versions of $x_1(n)$ and $x_2(n)$ by SU1. From the information theory perspective, the cases of $x_1(n) = \hat{x}_1(n)$ and $x_2(n) = \hat{x}_2(n)$ correspond to the source–relay channel not being in outage [33]. Then, based on (13) and (14), an error-free detection of these signals is possible if the following conditions are satisfied:

$$\frac{1-\tau}{2}W\log_2(1 + \gamma_{1,2|\nu}) \ge R_2, \tag{16}$$

$$\frac{1-\tau}{2}W\log_2(1 + \gamma_{1,1|\nu}) \ge R_1, \tag{17}$$

where R_1 and R_2 are the target data rates (in bits per second) for $x_1(n)$ and $x_2(n)$, respectively.

After decoding, during the second half of the transmission interval, SU_1 transmits $\hat{x}_2(n)$ to SU_2 with possible leakage to PU. Hence, the received signals at SU_2 and PU can be, respectively, written as

$$y_{2,2} = \sqrt{P_{r|\nu}}h_{12}\hat{x}_2(n) + n_{s2}(n), \tag{18}$$

$$y_{p,2} = \sqrt{P_{r|\nu}}h_{1p}\hat{x}_2(n) + \sqrt{P_p}h_{pp}\mu x_p(n) + n_p(n), \tag{19}$$

where $P_{r|\nu}$ is the transmission power of SU_1 under different $\widehat{H}_\nu$, and as before, $\mu \in \{0, 1\}$ defines the state of the PBS. With the help of (18), we can obtain the SNR of $\hat{x}_2(n)$ at SU_2 as

$$\gamma_{2|\nu} = \mid h_{12} \mid^2 \rho_{r|\nu}, \tag{20}$$

where we define $\rho_{r|\nu} = P_{r|\nu}/P_n$. Finally, the overall SINR received at SU_2 after maximum ratio combining (MRC) is given by

$$\gamma_{2,\mathrm{MRC}|\nu} = \gamma_{2,2|\nu} + \gamma_{2|\nu}\,. \tag{21}$$

In practice, the transmission by the SBS or SU_1 may create unacceptable levels of interference at PU. In many existing works (e.g. [23, 24]), the transmission power of the SUs is limited only by a pre-defined maximum value, which is not sufficient to protect the PU.

In this work, we use inequality constraints on the rate outage probability as a means to limit the interference of the SUs on PU. Specifically, let

$$P_{\mathrm{out}} = \Pr\Big\{\frac{1-\tau}{2}W\log_2\Big(1 + \frac{P_p \mid h_{pp} \mid^2}{I_{\mathrm{out}}^{\mathrm{PU}}}\Big) \le R_p\Big\}, \tag{22}$$

denote the rate outage probability at PU, where R_p is the target data rate, and $I_{\mathrm{out}}^{\mathrm{PU}}$ is the average interference level at PU. In order to protect PU, we demand that $P_{\mathrm{out}} \le P_{\mathrm{out}}^{\mathrm{PU}}$, where $P_{\mathrm{out}}^{\mathrm{PU}}$ is the maximum tolerable value of the outage probability. Since $|h_{pp}|^2$ obeys an exponential distribution with variance σ_{pp}^2, the interference threshold corresponding to a given level $P_{\mathrm{out}}^{\mathrm{PU}}$ can be obtained from (22) as

$$I_{\mathrm{out}}^{\mathrm{PU}} = -\frac{P_p\sigma_{pp}^2\ln\big(1 - P_{\mathrm{out}}^{\mathrm{PU}}\big)}{2^{\left(\frac{2R_p}{(1-\tau)W}\right)} - 1}. \tag{23}$$

With the help of (12) and (19), the interference power received at PU for different spectrum sensing events $(H_\mu, \widehat{H}_\nu)$ can be expressed as

$$I_{\mu\nu} = \begin{cases} P_{s\,|\,\nu}|h_{sp}|^2 + P_n, & \mu = 1, \\ P_n, & \mu = 0. \end{cases} \tag{24}$$

To protect the PU against interference from the SUs, therefore, the above interference power must not exceed the pre-defined threshold, i.e. $I_{\mu\nu} \le I_{\mathrm{out}}^{\mathrm{PU}}$. From the SUs' perspective (i.e. SBS or SU_1), the transmission power is further constrained by hardware and other limitations. Hence, by using (23) and (24), the transmission power of the SBS $P_{s|\nu}$ can be expressed as

$$P_{s|\nu} = \min\Big(\max\Big(\frac{I_{\mathrm{out}}^{\mathrm{PU}} - P_n}{\phi_{1\nu}\sigma_{sp}^2},\ 0\Big), P_s\Big), \tag{25}$$

and similarly, the transmission power of the SU_1 $P_{r|\nu}$ can be obtained as

$$P_{r|\nu} = \min\Big(\max\Big(\frac{I_{\mathrm{out}}^{\mathrm{PU}} - P_n}{\phi_{1\nu}\sigma_{12}^2},\ 0\Big), P_r\Big), \tag{26}$$

where P_s and P_r are the maximum transmission power of SBS and SU_1, respectively.

3 Outage performance analysis over Rayleigh fading channels with interference constraint

The outage probability is generally used as a performance metric for slow fading channels or real-time delay-sensitive applications. In this section, we consider a slow Rayleigh fading environment, where the channel coefficients remain constant during a time slot, and derive closed-form expressions of the outage probability for the traditional OMA and proposed NOMA-based schemes. When SU_1 and SU_2 transmit at constant rates R_1 and R_2, the outage probability is defined as the probability that the instantaneous SINR falls below a pre-defined threshold related to the target data rate [9].

3.1 Outage performance analysis for traditional OMA schemes

We separately consider the traditional OMA-I and OMA-II schemes as illustrated in Fig. 2.

3.1.1 OMA-I scheme.: As shown in Fig. 2*b*, this scheme uses time-division multiple access (TDMA) for the transmission of the SU signals at the SBS. Specifically, after the spectrum sensing phase, the SBS broadcasts the signal $x_{s1}(n) = \sqrt{P_{s|\nu}}x_1(n)$ during the first half of the transmission time interval, and then broadcasts the signal $x_{s2}(n) = \sqrt{P_{s|\nu}}x_2(n)$ during the second half. Since $|h_i|^2$ follows the exponential distribution with variance σ_i^2, the outage probabilities achieved by nodes SU_1 and SU_2 (i.e. $\sum_{\nu=0}^{1}\Pr(\widehat{H}_\nu)\Pr(|h_{sj}|^2 < u_j/\rho_{s|\nu})$) are given by

$$P_{\text{out},j}^{\text{OMA-I}} = \sum_{\nu=0}^{1}\Pr(\widehat{H}_\nu)\Big(1-\exp\big(-\frac{u_j}{\lambda_j}\big)\Big), \tag{27}$$

where $u_j = 2^{2R_j/((1-\tau)W)} - 1$ and $\lambda_j = \rho_{s|\nu}\sigma_{sj}^2$ for $j \in \{1,2\}$. Then the average outage probability of OMA-I can be expressed as

$$\begin{aligned} P_{\text{out}}^{\text{OMA-I}} &= \frac{1}{2}(P_{\text{out},1}^{\text{OMA-I}} + P_{\text{out},2}^{\text{OMA-I}}) \\ &= \frac{1}{2}\sum_{\nu=0}^{1}\Pr(\widehat{H}_\nu)\Big(2-\exp\big(-\frac{u_1}{\lambda_1}\big)-\exp\big(-\frac{u_2}{\lambda_2}\big)\Big). \end{aligned} \tag{28}$$

3.1.2 OMA-II scheme.: As shown in Fig. 2(c), the OMA-II scheme essentially amounts to DF relaying. Since the main benefit of NOMA over traditional cooperative communication (e.g. DF) is to allow multiple users to simultaneously share the same frequency band, it is important to compare its performance with OMA-II (i.e. traditional DF relaying) to demonstrate its effectiveness in terms of average outage probability and ergodic sum rate.

In OMA-II, after the spectrum sensing phase, the SBS broadcasts the signal $x_{s2}(n) = \sqrt{P_{s|\nu}}x_2(n)$ to SU_1 and SU_2 during the first half of the transmission time interval, and then SU_1 decodes $x_2(n)$ and forwards $\hat{x}_2(n)$ to SU_2 during the second half. Therefore, the overall outage event for SU_2 can be formulated as follows:

$$\Theta = \Theta_1 \cup \Theta_2, \tag{29}$$

where Θ_1 denotes the event that both SUs cannot decode $x_2(n)$ during the first half of the data transmission time interval, while Θ_2 denotes the event that $x_2(n)$ cannot be decoded successfully by SU_2 after MRC, while it can be decoded correctly by SU_1 during the first half of the transmission time interval. From these definitions, we can see that Θ_1 and Θ_2 are mutually exclusive. Thus, the outage probability of SU_2 is given by

$$P_{\text{out},2}^{\text{OMA-II}} = \Pr(\Theta_1) + \Pr(\Theta_2). \tag{30}$$

By introducing $\mathcal{I}_1 = \Pr\big(\rho_{s|\nu}|h_{s2}|^2 + \rho_{r|\nu}|h_{12}|^2 < u_2\big)$, $\Pr(\Theta_1)$ and $\Pr(\Theta_2)$ can be expressed as follows:

$$\begin{aligned} \Pr(\Theta_1) &= \sum_{\nu=0}^{1}\Pr(\widehat{H}_\nu)\Pr\Big(|h_{s1}|^2 < \frac{u_1}{\rho_{s|\nu}}\Big)\Pr\Big(|h_{s2}|^2 < \frac{u_2}{\rho_{s|\nu}}\Big) \\ &= \sum_{\nu=0}^{1}\Pr(\widehat{H}_\nu)\Big(1-\exp\Big(-\frac{u_1}{\lambda_1}\Big)\Big)\Big(1-\exp\Big(-\frac{u_2}{\lambda_2}\Big)\Big), \end{aligned} \tag{31}$$

and

$$\begin{aligned} \Pr(\Theta_2) &= \sum_{\nu=0}^{1}\Pr(\widehat{H}_\nu)\Pr\Big(|h_{s1}|^2 \geq \frac{u_1}{\rho_{s|\nu}}\Big)\mathcal{I}_1 \\ &= \sum_{\nu=0}^{1}\Pr(\widehat{H}_\nu)\exp\Big(-\frac{u_1}{\lambda_1}\Big)\mathcal{I}_1. \end{aligned} \tag{32}$$

Noting that $|h_{s2}|^2$ and $|h_{12}|^2$ are statistically independent and follow an exponential distribution, $\mathcal{I}_1$ can be calculated as

$$\mathcal{I}_1 = \begin{cases} 1-\exp\big(-\frac{u_2}{2\lambda_2}\big), & \lambda_2 = \lambda_3, \\ 1-\Omega_1\exp\big(-\frac{u_2}{\lambda_2}\big)+\Omega_2\exp\big(-\frac{u_2}{\lambda_3}\big), & \lambda_2 \neq \lambda_3, \end{cases} \tag{33}$$

where $\lambda_3 = \rho_{r|\nu}\sigma_{12}^2$, $\Omega_1 = \lambda_2/(\lambda_3-\lambda_2)$ and $\Omega_2 = 1-\Omega_1 = \lambda_3/(\lambda_3-\lambda_2)$. Since the SBS does not transmit SU_1's signal in the OMA-II scheme, we assume the outage probability of SU_1 to be 1, i.e. $P_{\text{out},1}^{\text{OMA-II}} = 1$. Then, the average outage probability of OMA-II can be expressed as

$$P_{\text{out}}^{\text{OMA-II}} = \frac{1}{2}\big(P_{\text{out},1}^{\text{OMA-II}} + P_{\text{out},2}^{\text{OMA-II}}\big). \tag{34}$$

3.2 Outage performance analysis for NOMA-based transmission scheme

Based on the preliminary results on detection performance and transmission power level derived in Section 2, the outage probability of SU_1 can be expressed as

$$P_{\text{out},1}^{\text{NOMA}} = \sum_{\nu=0}^{1}\Pr(\widehat{H}_\nu)\Big(1-\underbrace{\Pr(\gamma_{1,1|\nu}\geq u_1)}_{\mathcal{I}_{11}}\underbrace{\Pr(\gamma_{1,2|\nu}\geq u_2)}_{\mathcal{I}_{12}}\Big), \tag{35}$$

where $\mathcal{I}_{11}$ and $\mathcal{I}_{12}$ denote the probabilities that SU_1 can decode $x_1(n)$ and $x_2(n)$ correctly, respectively. Based on (13) and (14), we obtain

$$\mathcal{I}_{11} = \Pr\Big(|h_{s1}|^2 \geq \frac{u_1}{\alpha_1\rho_{s|\nu}}\Big) = \exp\Big(-\frac{u_1}{\alpha_1\lambda_1}\Big), \tag{36}$$

$$\mathcal{I}_{12} = \Pr\Big(|h_{s1}|^2 \geq \frac{\omega}{\rho_{s|\nu}}\Big) = \begin{cases} 0, & u_2 \geq \frac{\alpha_2}{\alpha_1}, \\ \exp\big(-\frac{\omega}{\lambda_1}\big), & u_2 < \frac{\alpha_2}{\alpha_1}, \end{cases} \tag{37}$$

where $\omega = u_2/(\alpha_2 - u_2\alpha_1)$. When $u_2 \geq \alpha_2/\alpha_1$, $P_{\text{out},1}^{\text{NOMA}} = 1$. Hence, it is necessary to have $u_2 < \alpha_2/\alpha_1$, which is the same constraint as that in [9].

Next, we characterise the outage probability achieved by SU_2. We first note that the overall outage event for SU_2 can be expressed as in (29), i.e. $\Theta' = \Theta_1' \cup \Theta_2'$, with Θ_1' and Θ_2' defined in a similar manner as in the OMA-I scheme.

Therefore, the outage probability of SU_2 can be expressed as

$$P_{\text{out},2}^{\text{NOMA}} = \Pr(\Theta_1') + \Pr(\Theta_2'), \tag{38}$$

where $\Pr(\Theta_1')$ and $\Pr(\Theta_2')$ are given by

$$\Pr(\Theta_1') = \sum_{\nu=0}^{1} \Pr(\widehat{H}_\nu)\Pr(\gamma_{1,2|\nu} < u_2)\Pr(\gamma_{2,2|\nu} < u_2), \tag{39}$$

$$\Pr(\Theta_2') = \sum_{\nu=0}^{1} \Pr(\widehat{H}_\nu)\Pr(\gamma_{1,2|\nu} \geq u_2)\Pr(\gamma_{2,\mathrm{MRC}|\nu} < u_2). \tag{40}$$

Proposition 1: The closed-form expression for the probability of Θ_1' is given by

$$\Pr(\Theta_1') = \begin{cases} 1, & u_2 \geq \dfrac{\alpha_2}{\alpha_1}, \\ \displaystyle\sum_{\nu=0}^{1} \Pr(\widehat{H}_\nu)\Big(1 - \exp\Big(-\frac{\omega}{\lambda_1}\Big)\Big) & \\ \quad \cdot \Big(1 - \exp\Big(-\frac{\omega}{\lambda_2}\Big)\Big), & u_2 < \dfrac{\alpha_2}{\alpha_1}, \end{cases} \tag{41}$$

while the approximate closed-form expression for the probability of Θ_2' is given by

$$\Pr(\Theta_2') \simeq \begin{cases} 0, & u_2 \geq \dfrac{\alpha_2}{\alpha_1}, \\ \displaystyle\sum_{\nu=0}^{1} \Pr(\widehat{H}_\nu)\exp\Big(-\frac{\omega}{\lambda_1}\Big)\Big(1 - \exp\Big(-\frac{\omega}{\lambda_2}\Big) & \\ -u_2\Omega_3\exp\Big(-\frac{u_2}{\lambda_3}\Big)\Big), & u_2 < \dfrac{\alpha_2}{\alpha_1}, \end{cases} \tag{42}$$

where

$$\Omega_3 = \frac{\pi}{2(n+1)} \sum_{k=0}^{K} \frac{\alpha_2\sqrt{(1-x_k^2)}}{\lambda_2(\alpha_2 - \alpha_1 y_k)^2} \exp\Big(\frac{y_k}{\lambda_3} - \frac{y_k}{\lambda_2(\alpha_2 - \alpha_1 y_k)}\Big),$$

$$x_k = \cos\frac{(2k+1)\pi}{2(K+1)},$$

$$y_k = \frac{u_2}{2}(x_k + 1), \quad k \in \{0, 1, \ldots, K\}$$

and K is a Gaussian–Chebyshev parameter [34, eq.(25.4.38)].

Proof: See Appendix. □

It is clear from (41) and (42) that the outage probability of SU_2 in the proposed NOMA scheme increases with increasing P_f and τ or decreasing P_s and P_r. This is because the amount of time or power devoted to the secondary transmission is reduced.

Finally, the average outage probability of the proposed NOMA scheme can be expressed as

$$P_{\mathrm{out}}^{\mathrm{NOMA}} = \frac{1}{2}\Big(P_{\mathrm{out},1}^{\mathrm{NOMA}} + P_{\mathrm{out},2}^{\mathrm{NOMA}}\Big). \tag{43}$$

To summarise, the average outage probabilities for the OMA-I, OMA-II and the proposed NOMA schemes are given by (28), (34) and (43), respectively. It is obvious that the average outage probability increases with increasing P_f and τ. Hence, determining an appropriate value of τ is essential for practical designs, especially when the average outage probability of the SUs is under control.

4 Ergodic sum rate analysis over Rayleigh fading channels with interference constraint

In contrast to the outage probability studied in the previous section, the ergodic rate provides a more appropriate metric for fast fading channels or delay-insensitive applications. Hence, in this section, we consider a fast fading Rayleigh environment, where signals transmitted at different times n may experience different fading states of the channel, and characterise the performance of the OMA-I, OMA-II and proposed NOMA-based transmission schemes in terms of their ergodic sum rates.

4.1 Ergodic sum rate analysis for traditional OMA schemes

4.1.1 OMA-I scheme.: On the condition that SU_j can detect the sequence of symbols $x_j(n)$ for $j \in \{1, 2\}$, the ergodic rate associated with $x_j(n)$ is then given by

$$\begin{aligned} R_j^{\mathrm{OMA-I}} &= \frac{1-\tau}{2} W \sum_{\nu=0}^{1} \Pr(\widehat{H}_\nu)\mathbb{E}[\log_2(1 + \rho_{s|\nu}|h_{sj}|^2)] \\ &= \frac{1-\tau}{2\ln 2} W \sum_{\nu=0}^{1} \Pr(\widehat{H}_\nu) \int_0^\infty \frac{1 - F_{\mathrm{X}}(x)}{1+x} dx, \end{aligned} \tag{44}$$

where we have introduced random variable $\mathrm{X} = \rho_{s|\nu}|h_{sj}|^2$ with $F_{\mathrm{X}}(x) = 1 - \exp(-\frac{x}{\lambda_j})$. Based on [35, eq.(3.352.4)], $R_j^{\mathrm{OMA-I}}$ is obtained as

$$R_j^{\mathrm{OMA-I}} = -\frac{1-\tau}{2\ln 2} W \sum_{\nu=0}^{1} \Pr(\widehat{H}_\nu)\exp\Big(\frac{1}{\lambda_j}\Big)\mathrm{Ei}\Big(-\frac{1}{\lambda_j}\Big), \tag{45}$$

where $\mathrm{Ei}(\cdot)$ denotes the exponential integral function [35, eq. (8.211.1)].

Based on the above equation, the ergodic sum rate of OMA-I is then obtained as

$$R^{\mathrm{OMA-I}} = R_1^{\mathrm{OMA-I}} + R_2^{\mathrm{OMA-I}}. \tag{46}$$

4.1.2 OMA-II scheme.: We first note that for DF relaying, the end-to-end rate is essentially limited by the weakest link. Hence, by introducing $\mathrm{Y} = \min\left\{\rho_{s|\nu}|h_{s1}|^2, \rho_{s|\nu}|h_{s2}|^2 + \rho_{r|\nu} \mid h_{12}\mid^2\right\}$, the ergodic rate of $x_2(n)$ in the OMA-II scheme can be expressed as

$$\begin{aligned} R_2^{\mathrm{OMA-II}} &= \frac{1-\tau}{2} W \sum_{\nu=0}^{1} \Pr(\widehat{H}_\nu)\mathbb{E}[\log_2(1 + \mathrm{Y})] \\ &= \frac{1-\tau}{2\ln 2} W \sum_{\nu=0}^{1} \Pr(\widehat{H}_\nu) \int_0^\infty \frac{1 - F_{\mathrm{Y}}(y)}{1+y} \mathrm{d}y. \end{aligned} \tag{47}$$

With the help of (33), $F_{\mathrm{Y}}(y)$ can be obtained as

$$F_{\mathrm{Y}}(y) = \begin{cases} 1 - \exp(-\lambda_4 y), & \lambda_2 = \lambda_3, \\ 1 - \Omega_1\exp(-\lambda_5 y) - \Omega_2\exp(-\lambda_6 y), & \lambda_2 \neq \lambda_3, \end{cases} \tag{48}$$

where

$$\lambda_4 = \frac{1}{\lambda_1} + \frac{1}{2\lambda_2}, \quad \lambda_5 = \frac{1}{\lambda_1} + \frac{1}{\lambda_2} \quad \text{and} \quad \lambda_6 = \frac{1}{\lambda_1} + \frac{1}{\lambda_3}.$$

Based on (47), (48) and [35, eq.(3.352.4)], the ergodic sum rate of OMA-II is obtained as

$$R^{\mathrm{OMA-II}} = \begin{cases} -\dfrac{1-\tau}{2\ln 2} W \displaystyle\sum_{\nu=0}^{1} \Pr(\widehat{H}_\nu)\exp(\lambda_4)\mathrm{Ei}(-\lambda_4), & \lambda_2 = \lambda_3, \\ -\dfrac{1-\tau}{2\ln 2} W \displaystyle\sum_{\nu=0}^{1} \Pr(\widehat{H}_\nu)[\Omega_1\exp(\lambda_5)\mathrm{Ei}(-\lambda_5) & \\ \quad + \Omega_2\exp(\lambda_6)\mathrm{Ei}(-\lambda_6)], & \lambda_2 \neq \lambda_3 \end{cases} \tag{49}$$

4.2 Ergodic sum rate analysis for NOMA-based transmission scheme

On the condition that sequence $x_1(n)$ can be decoded at SU_1 after SIC, the ergodic rate associated with $x_1(n)$ is given by

$$R_1^{\mathrm{NOMA}} = \frac{1-\tau}{2} W \sum_{\nu=0}^{1} \Pr(\widehat{H}_\nu)\mathbb{E}[1+\gamma_{1,1|\nu}] = -\frac{1-\tau}{2\ln 2} W \sum_{\nu=0}^{1} \Pr(\widehat{H}_\nu)\exp\Big(\frac{1}{\alpha_1\lambda_1}\Big)\mathrm{Ei}\Big(-\frac{1}{\alpha_1\lambda_1}\Big). \tag{50}$$

We note that sequence $x_2(n)$ should be detected at SU_2 as well as at SU_1 for SIC to be effective. Hence, by introducing $\mathrm{Z} = \min\{\gamma_{1,2|\nu}, \gamma_{2,\mathrm{MRC}|\nu}\}$, the ergodic rate of $x_2(n)$ for NOMA can be expressed as

$$R_2^{\mathrm{NOMA}} = \frac{1-\tau}{2} W \sum_{\nu=0}^{1} \Pr(\widehat{H}_\nu)\mathbb{E}[\log_2(1+\mathrm{Z})] = \frac{1-\tau}{2\ln 2} W \sum_{\nu=0}^{1} \Pr(\widehat{H}_\nu) \int_0^\infty \frac{1-F_{\mathrm{Z}}(z)}{1+z}\,\mathrm{d}z. \tag{51}$$

With the help of (42), $F_{\mathrm{Z}}(z)$ can be rewritten as

$$F_{\mathrm{Z}}(z) = 1 - \Pr(\gamma_{1,2|\nu} > z)\Pr(\gamma_{2,\mathrm{MRC}|\nu} > z) = \begin{cases} 1, & z \geq \dfrac{\alpha_2}{\alpha_1}, \\ 1 - \exp(-\lambda_4\omega_1) - \Omega_4 z \exp\Big(-\dfrac{z}{\lambda_3} - \dfrac{\omega_1}{\lambda_1}\Big), & z < \dfrac{\alpha_2}{\alpha_1}, \end{cases} \tag{52}$$

where

$$\Omega_4 = \frac{\pi}{2(n+1)} \sum_{k=0}^{K} \frac{\alpha_2\sqrt{(1-x_k^2)}}{\lambda_2(\alpha_2-\alpha_1 z_k)^2} \exp\Big(\frac{z_k}{\lambda_3} - \frac{z_k}{\lambda_2(\alpha_2-\alpha_1 z_k)}\Big),$$

$$\omega_1 = \frac{z}{\alpha_2 - z\alpha_1}$$

and

$$z_k = \frac{z}{2}(x_k+1) \quad \text{for} \quad k \in \{0,1,2,\ldots,K\}.$$

Then, by substituting (52) into (50), the ergodic rate of $x_2(n)$ can be expressed as

$$R_2^{\mathrm{NOMA}} = \frac{1-\tau}{2\ln 2} W \sum_{\nu=0}^{1} \Pr(\widehat{H}_\nu) \int_0^{\frac{\alpha_2}{\alpha_1}} \Big(\frac{1}{1+z}\exp(-\lambda_4\omega_1) + \frac{\Omega_4 z}{1+z}\exp\Big(-\frac{z}{\lambda_3} - \frac{\omega_1}{\lambda_1}\Big)\Big)\mathrm{d}z. \tag{53}$$

While it does not appear possible to express the above integral in closed form, its numerical evaluation is straightforward so that the value of R_2^{NOMA} can be easily calculated from (53) using one-dimensional numerical integration.

From (50) and (53), the ergodic sum rate of NOMA is finally obtained as

$$R^{\mathrm{NOMA}} = R_1^{\mathrm{NOMA}} + R_2^{\mathrm{NOMA}}. \tag{54}$$

In summary, the ergodic sum rate for the OMA-I, OMA-II and the proposed NOMA schemes are given by (46), (49) and (54), respectively. Clearly, these three equations exhibit a complex non-linear nature in their various parameters and it is very difficult to obtain a closed-form expression for the optimal value of τ, denoted as τ^*, that maximises the ergodic sum rate. Thus, we will use a numerical approach to obtain τ^* for each choice of parameter values in the following section.

5 Practical considerations

In this section, we provide some discussions about the impacts of imperfect CSI, interference cancellation residual errors in SIC and the possible extension of our work to multiple antennas SBS to make our approach more valuable in practical applications.

5.1 Imperfect CSI

For many practical transmission scenarios, the transmitter nodes are usually aware of the number and identity of the receiving nodes. The CSI between the different nodes can then be obtained via the application of established channel estimation methods, although this estimation will entail errors [23]. Here, by using the minimum mean square channel estimation error model [36], the estimated Rayleigh fading channel coefficients $\hat{h}_i$, where $i \in \{\mathrm{pp}, \mathrm{ps}, \mathrm{sp}, \mathrm{s1}, \mathrm{s2}, 12, 1\mathrm{p}\}$, can be modelled as

$$\hat{h}_i = h_i + e_i, \tag{55}$$

where h_i is the true channel modelled as in Section 2.1, and $e_i \sim \mathcal{CN}(0, \sigma_e^2)$ is the estimated error with variance σ_e^2. Considering imperfect CSI, the transmitter nodes only have access to the estimated fading channel coefficients $\hat{h}_i$ instead of the true channel gains h_i.

To assess the effect of the estimated errors e_i on the outage probability measures developed in this work, we will conduct Monte Carlo simulations in Section 6.4 where both the estimated gains $\hat{h}_i$ modelled as above, and their true values h_i are used to evaluate various outage probabilities.

5.2 Imperfect SIC

In this case, we suppose that the signal from SU_2 (i.e. $x_2(n)$) cannot be perfectly removed at SU_1 because of SIC error propagation which will entail residual interference. In general, the residual interference caused by imperfect SIC is a complicated function of multiple factors, e.g. coding parameters, the type of SIC employed, channel model and user mobility conditions. As a first attempt to model the impact of imperfect SIC, we adopt the linear model of error propagation in the proposed CRN system in this work (see also [37, 38]).

Under this model, the SINR of $x_1(n)$ at SU_1 can be rewritten as

$$\gamma_{1,1|\nu}^e = \alpha_1 \mid h_{\mathrm{s1}} \mid^2 \rho_{s|\nu}^e = \frac{\alpha_1 \mid h_{\mathrm{s1}} \mid^2 P_{s|\nu}}{P_n + I_{2,1}^e}, \tag{56}$$

where $\rho_{s|\nu}^e = P_{s|\nu}/(P_n + I_{2,1}^e)$, $I_{2,1}^e = \alpha_1 \mid h_{\mathrm{s1}} \mid^2 \mid e_{2,1} \mid^2$ is the interference resulting from imperfect cancellation of $x_2(n)$ at SU_1 during SIC and $e_{2,1} = x_2(n) - \hat{x}_2(n)$ is the difference between the decoded signal (i.e. $\hat{x}_2(n)$) and actual signal (i.e. $x_2(n)$). Then, we model the SIC error as $e_{2,1} \sim \mathcal{CN}(0, \sigma_{e1}^2)$ and thus, $\mid e_{2,1} \mid^2$ is a random variable with a chi-squared distribution with two degrees of freedom.

To assess the effects of the SIC errors $e_{2,1}$ on the values of $P_{\mathrm{out},1}^{\mathrm{NOMA}}$ and R_1^{NOMA} developed in this work, we will conduct Monte Carlo simulations in Section 6.4 where both $\gamma_{1,1|\nu}^e$ modelled in (56) as above, and its ideal value $\gamma_{1,1|\nu}$ under perfect SIC are used to evaluate the outage probability and ergodic rate of SU_1.

5.3 Extension to multiple antenna base station

As an example, we consider a downlink cognitive NOMA transmission scenario with a single SBS that serves a set K SUs. The SUs are uniformly distributed within a circle, while the SBS equipped with M antennas is located at the centre of this circle. The channel coefficients between the SBS antennas and the kth SU (i.e. SU_k) denoted by $h_{m,k}$, where m is the antenna index, are modelled as mutually independent complex random variables with Rayleigh fading distribution where $k \in \{1,2,\ldots,K\}$ and $m \in \{1,2,\ldots,M\}$.

For each antenna, the SUs are sorted based on their channel gains in decreasing order, i.e. $|h_{m,1}|^2 > |h_{m,2}|^2 > \cdots > |h_{m,K}|^2$. The receiver of user k aims to cancel the interference from any other

Table 1 Simulation parameters

Simulation parameter	Value
time slot duration: T	10 ms
sampling frequency: f_s	50 kHz
spectrum sensing time fraction: τ	0.1
target false alarm probability: P_f	0.1
power ratio: ρ_p	−10, 10 dBm
variance of channel SBS-SU_2: σ_{s2}^2	0.04
variances of other channels: σ_{pp}^2, σ_{ps}^2 σ_{s1}^2, σ_{12}^2, σ_{sp}^2 and σ_{1p}^2	1
probability for the licensed channel to be on: p	0.4
power allocation coefficient of SU_1: α_1	0.3
target data rates for $x_1(n)$, $x_2(n)$ and $x_p(n)$: R_1, R_2 and R_p	7.5 kbps
Gaussian noise variance: P_n	1
outage probability requirement of PU: P_{out}^{PU}	0.1
maximum transmission power of SBS and SU_1: $P_s = P_r$	23 dBm
Gaussian-Chebyshev parameter: K	10
number of Monte Carlo runs	10,000

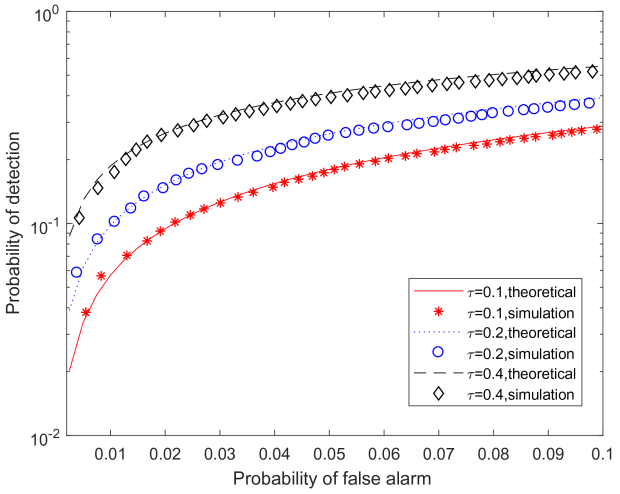

Fig. 3 *Probability of detection versus probability of false alarm for different values of* τ ($\rho_p = -10$dBm)

users whose index is greater than k using SIC, while the remaining SUs' signals with indices lower than k, are treated as interference. Thus, the SINR of $x_{k'}(n)$ at SU_k via the mth SBS antenna can be expressed as

$$\gamma_{k,k'|\nu}^{m} = \frac{\alpha_{k'}^{m} \mid h_{m,k} \mid^2 P_{s|\nu}}{P_n + P_{s|\nu} \mid h_{m,k} \mid^2 \sum_{j=1}^{k'-1} \alpha_j^m + I_{k,k'}^e}, \quad (57)$$

where $\alpha_k^m > 0$ is the power allocation coefficient for the kth SU at the mth antenna with $\sum_{j=1}^{K} \alpha_j^m = 1$ and $\alpha_1^m \le \alpha_2^m, \ldots, \le \alpha_K^m$. Moreover, $I_{k,k'}^e$ is the interference resulting from imperfect cancellation during SIC, which in the presence of random SIC errors can be expressed as $I_{k,k'}^e = P_{s|\nu} \mid h_{m,k} \mid^2 \sum_{j=k+1}^{K} \alpha_j^m \mid e_{j,k} \mid^2$. As can be seen from (57), the power allocation α_K^m and the channel coefficients $h_{m,k}$ will now jointly impact the determination of the outage probability and ergodic sum rate in the multiple antennas scenario.

5.4 Applications

The proposed NOMA-based cooperative relaying scheme can be used not only in CRN framework, but also in existing and other future wireless systems because of its compatibility with communication systems design.

Firstly, we take 5G wireless networks as an example, a balanced trade-off between fairness and smart devices' requirements could be achieved by our proposed scheme to meet the demand of massive connectivity for the 5G, where PUs and/or SUs using distinct devices can be served simultaneously on the same shared band with different power level. Specifically, we suppose a scenario that the BS needs to serve the mth user (i.e. viewed as a PU) via channel p, while the proposed NOMA scheme can be implemented within two users (i.e, viewed as SU_1 and SU_2 as a group) which opportunity admitted into the channel p with limited performance degradation to mth user. According to this system, SUs have an equal chance to utilise the same bandwidth resource, and one selected SU with weaker channel gain but stronger demand of data rate (e.g. SU_2) is allocated with more power to fulfill predefined QoS requirements.

Furthermore, the proposed scheme in CRN can also be applied to heterogeneous 5G networks in which a macro-cell interoperates with multiple smaller cells, in order to achieve high spectral efficiency. Thus, based on the results obtained in this work, it is expected that the NOMA-based transmission relaying between multiple small cells within a macro-cell can achieve additional capacity gain, which remains an interesting avenue for future work.

6 Simulation results

In this section, the outage probabilities and ergodic rates of the three different schemes are evaluated by means of computer simulations. The default values (or range of values) of all the relevant simulation parameters are summarised in Table 1 (see also [16, 21]).

6.1 Detection probability

We compare the values of detection and false alarm probabilities, i.e. P_d and P_f, obtained from the Monte Carlo simulations to the theoretical results derived in Section 2. In the simulations, we first determine the detection threshold θ needed to achieve the target P_f under H_0, and then apply this threshold to obtain P_d. Fig. 3 shows the comparison between the results of Monte Carlo simulations and theoretical probability calculation based on (6) for $P_f \in [0, 0.1]$ and $\rho_p = -10$ dBm, and for different values of τ. It is observed that for a given value of P_f, P_d increases with τ, while for a given P_d, P_f decreases as τ increases. This result is easy to understand since when τ increases, additional observations become available which help reduce the variance of the energy estimator in (6), and in turn improve the detection performance.

6.2 Outage probability

Fig. 4 shows the outage probability of the SUs (i.e. SU_1 and SU_2) versus probability of false alarm P_f for the OMA-I, OMA-II and proposed NOMA schemes, as obtained from simulations and theoretical analysis. One can see a close match between the outage probability values obtained by Monte Carlo simulation and the corresponding analytical results derived in (27), (30), (35) and (38). It is also clear that the outage probability of the OMA-I, OMA-II and proposed NOMA schemes increase with increasing P_f. This is because the transmission time or power devoted to the secondary transmission is reduced in proportion. Besides, it is seen that the OMA-I scheme achieves a lower outage probability than the other schemes for SU_1. This is because more power is allocated to SU_1 in the OMA-I scheme (i.e. $P_{s|\nu}$ for OMA-I versus $\alpha_1 P_{s|\nu}$ for the NOMA scheme), and the available transmission power dominates the outage probability in this case. It is also noted that OMA-II achieves a lower outage probability than other schemes for SU_2. This can be explained by the fact that with OMA-II, more time is allocated to the transmission of SU_2's signal (i.e. second half of transmission interval only for OMA-I, versus whole transmission interval for OMA-II and NOMA). Compared with the NOMA scheme, more power is allocated to SU_2 in OMA-II (i.e. $P_{s|\nu}$ for OMA-II and $\alpha_2 P_{s|\nu}$ for the NOMA scheme), and the available transmit time and power dominate the outage probability in this case. Futhermore, although the NOMA scheme does not

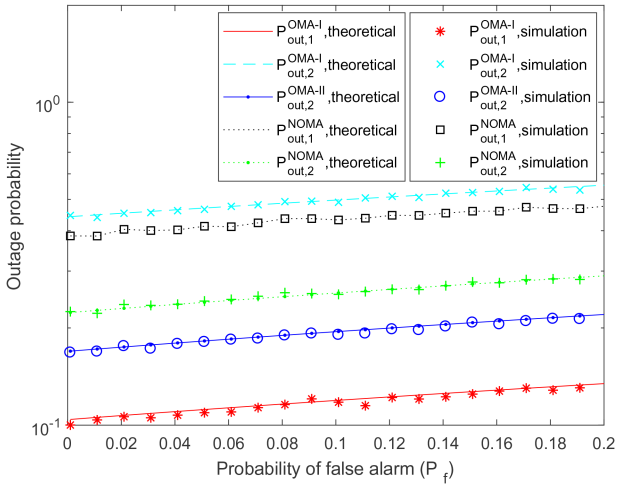

Fig. 4 *Outage probability versus probability of false alarm ($\rho_p = 10$ dBm)*

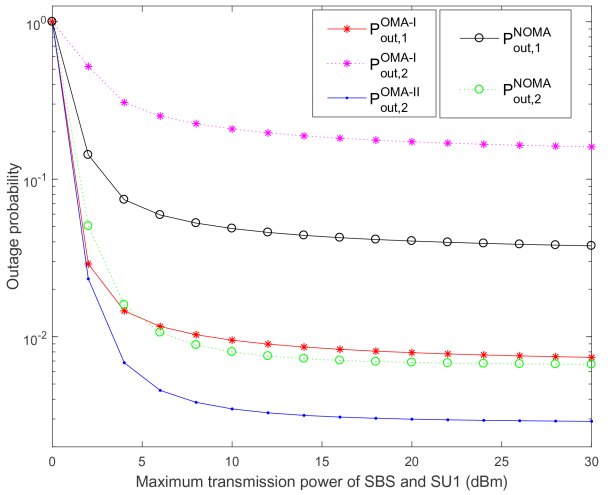

Fig. 5 *Outage probability versus maximum transmission power of SBS and* SU_1 *($\rho_p = 10$ dBm)*

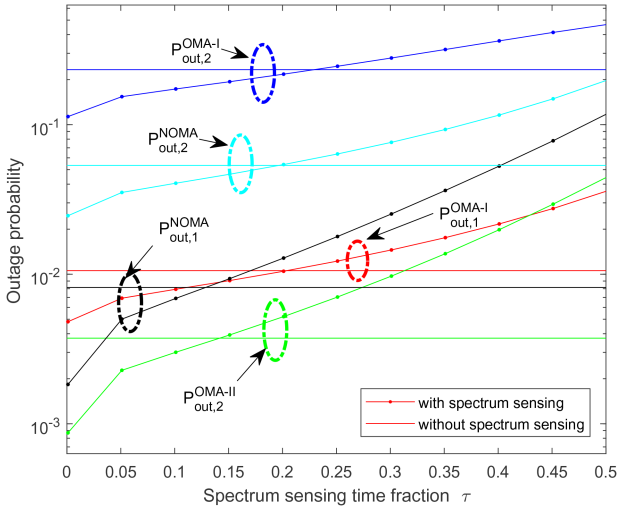

Fig. 6 *Outage probability versus spectrum sensing time fraction*

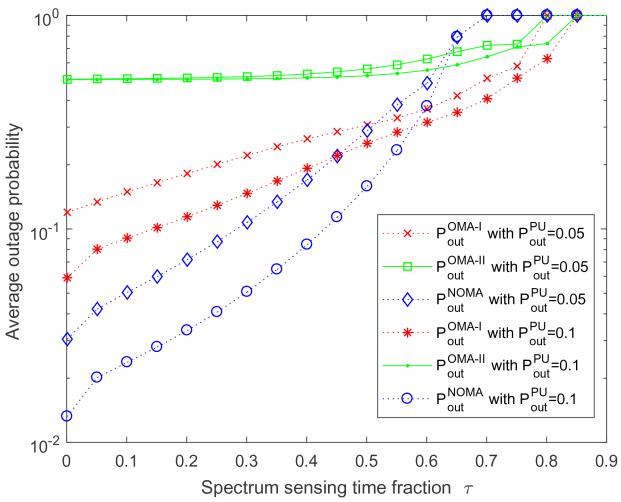

Fig. 7 *Average outage probability versus spectrum sensing time fraction for different values of $P_{\text{out}}^{\text{PU}}$ ($\rho_p = 10$ dBm)*

achieve the best outage probability for SU_1 and SU_2, it will achieve the best average outage probability, as shown below.

Fig. 5 shows the outage probability of SU_1 and SU_2 versus the maximum transmission power of SBS and SU_1 (i.e. P_s and P_r) for the three schemes under consideration, as obtained from simulations and theory. From this figure, it is seen that the outage probabilities of SU_1 and SU_2 decrease with an increase in P_s and P_r, especially in the low power region. However, in the high power regions, the outage probability is dominated by P_d and P_f which are independent of P_s and P_r, hence the outage probability flattens to a lower limit.

In Fig. 6, we show the theoretical outage probability of the two SUs versus the sensing time fraction τ for the three schemes under study, as well as the outage probability of the traditional underlay CRN transmission schemes (i.e. without spectrum sensing). We first note that the outage probability of the OMA-I, OMA-II and proposed NOMA schemes increase with increasing τ, since the transmission time is reduced in proportion. The outage probability of the traditional underlay CRN transmission schemes are constant since they do not employ spectrum sensing. Importantly, we note that the outage probability of the OMA-I, OMA-II and NOMA schemes is smaller than that of the corresponding traditional scheme when the value of τ is kept small (e.g, $\tau < 0.12$ for NOMA). Hence, determining an appropriate value of τ is essential to improve the outage performance for the proposed system.

In Fig. 7, we show the average theoretical outage probability of the SUs versus the sensing time fraction τ for the three schemes under study, as obtained from (28), (34) and (43), and for different values of the outage probability at the PU (i.e. $P_{\text{out}}^{p} = 0.05$ and 0.1).

From this figure, one can see that the average outage probability increases with an increase in τ or a decrease in P_{out}^{p}. Especially, when τ is larger than 0.7, the average outage probabilities becomes quite large. Indeed, the average outage probability for the three schemes is mainly dependent on the transmission time and power. As τ increases or P_{out}^{p} decreases, the amount of time or power devoted to the secondary transmission is reduced, leading to an increase in the average outage probability. Besides, simulation results show that NOMA can outperform the OMA schemes in terms of outage probability especially for smaller values of the sensing time (i.e. $\tau < 0.5$).

In Fig. 8, we show the average theoretical outage probabilities of the SUs versus τ for different values of the SBS-SU_2 channel variance (i.e. $\sigma_{s2}^2 \in \{0.04, 0.25\}$), which provides a measure of the link quality. It is seen that for a given τ, σ_{s2}^2 strongly affects the performance of OMA-I. In particular, as the quality of the SBS-SU_2 link increases, with σ_{s2}^2 reaching 0.25, the performance of OMA-I now slightly exceeds that of NOMA. In general however, we find that the NOMA scheme can achieve a better outage performance than the traditional OMA schemes especially when the SBS-SU_2 link is in bad condition.

In Fig. 9, we show the average theoretical outage probability of the SUs for NOMA versus SU_1's power allocation coefficient α_1, for different values of τ (i.e. $\tau \in \{0.1, 0.2, 0.5\}$). In our simulations, we choose the range of α_1 from 0 to 0.5 (since $\alpha_1 + \alpha_2 = 1$ and $\alpha_1 \leq \alpha_2$), and it is seen that for a given τ, the average outage probability curve exhibits a 'U' shape with a unique minimum. Then, we use a numerical approach to obtain the optimal values of

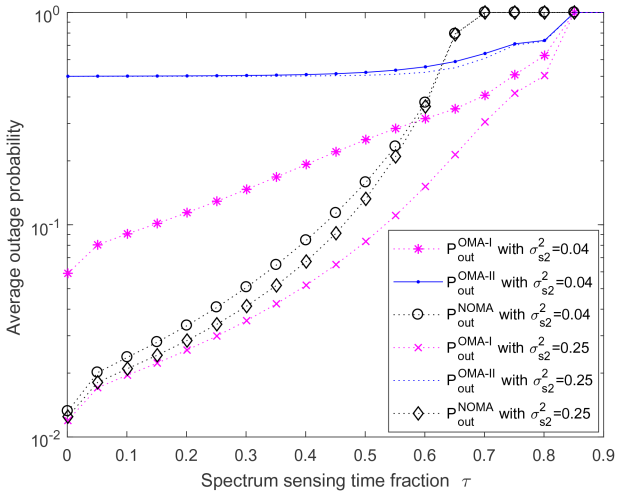

Fig. 8 *Average outage probability versus spectrum sensing time fraction for different values of* σ_{s2}^2 *(*$\rho_p = 10$ dBm*)*

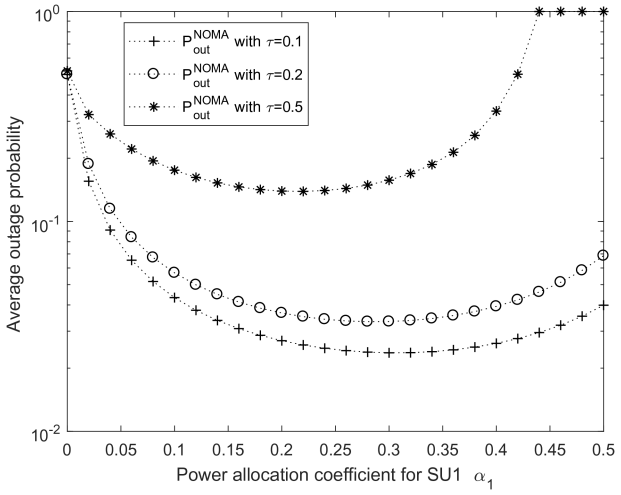

Fig. 9 *Average outage probability versus power allocation coefficient of* SU_1 *for different values of* τ *(*$\rho_p = 10$ dBm*)*

Table 2 Optimal values power allocation coefficient α_1^* for different target data rates R_1 and R_2

(R_1, R_2)	α_1^*	(R_1, R_2)	α_1^*
(7.5, 7.5)	0.3	(7.5,5)	0.4
(12.5,7.5)	0.36	(7.5,12.5)	0.2
(17.5,7.5)	0.4	(7.5,17.5)	0.14

α_1 (i.e. α_1^*) for $\tau = 0.1$, 0.2 and 0.5. For the particular system configuration under evaluation here, the values of α_1^* are approximately equal to 0.30, 0.28 and 0.22, respectively. In general, we have found that the optimal α_1^* is inversely proportional to τ. We list the optimal α_1^* for different choices of the target data rates R_1 and R_2 intended for the user signals $x_1(n)$ and $x_2(n)$ (see (16) and (17)) in Table 2. As observed, with an increase in R_1 or a decrease in R_2, more power is needed for SU_1's transmission, leading to the increase of α_1^*.

6.3 Ergodic rate

In Fig. 10, we show the ergodic rate of the three schemes versus P_f, as obtained from simulations and theoretical analysis. We can find a close match between the values obtained by Monte Carlo simulation and the corresponding analytical results derived in (45), (49), (50) and (53). It is also noted that the ergodic rate of the three schemes decrease with increasing P_f, due to the reduced transmission time or power devoted to SBS and SU1. Besides, it is

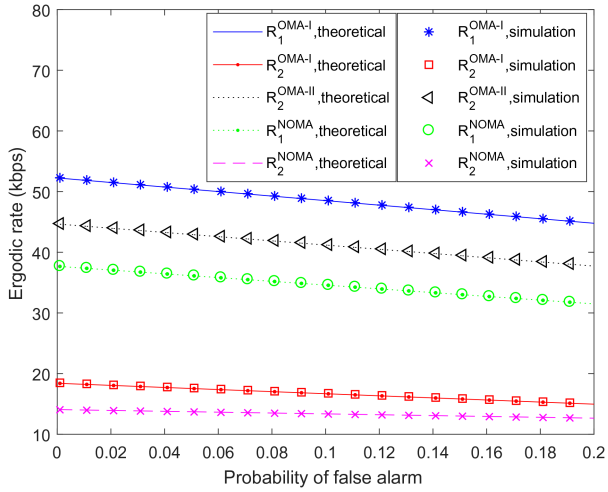

Fig. 10 *Ergodic rate versus probability of false alarm (*$\rho_p = 10$ dBm*)*

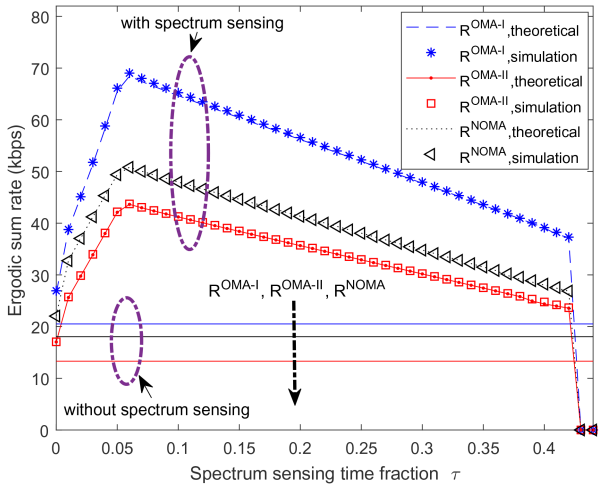

Fig. 11 *Ergodic rates versus spectrum sensing time fraction (*$\rho_p = 10$ dBm*)*

seen that the maximum ergodic rates of $x_1(n)$ and $x_2(n)$ are, respectively, achieved by the OMA-I and OMA-II schemes. This can be explained by the fact that more power is allocated to SU_1 in the OMA-I scheme, while more transmission time is allocated to SU_2 in OMA-II.

In Fig. 11, we show the ergodic sum rate of the three schemes versus τ, and that of the traditional underlay CRN schemes as a benchmark. As observed, there is a close match between the values obtained by simulations and the corresponding analytical results based on (46), (49) and (54). In addition, the ergodic sum rate of the traditional schemes is constant (since they are independent of the spectrum sensing time), and is always smaller than that of OMA-I, OMA-II and the proposed NOMA schemes. More importantly, we generally find that for the latter schemes, there exists an optimal spectrum sensing time fraction (i.e. τ^*) which maximises the ergodic sum rate. However, the analytical expressions in (46), (49) and (54) are complex and non-linear, and it is very difficult to obtain a closed-form expression for the optimal value of τ^* maximising the ergodic sum rate. In our simulations, we use a numerical approach to obtain τ^* for each choice of parameter values. For the particular system configuration under evaluation here, the value of τ^* for the three schemes is approximately equal to 0.06.

We should emphasise that the proposed NOMA and OMA-II schemes are both based on DF relaying, while OMA-I employs TDMA without cooperation. It is therefore not surprising that the ergodic sum rate of OMA-I exceeds that of NOMA and OMA-II, since the DF relay (i.e. SU_1) sacrifices transmission time and power to improve the outage performance of the distant user (i.e. SU_2). However, the ergodic sum rate of NOMA exceeds that of OMA-II,

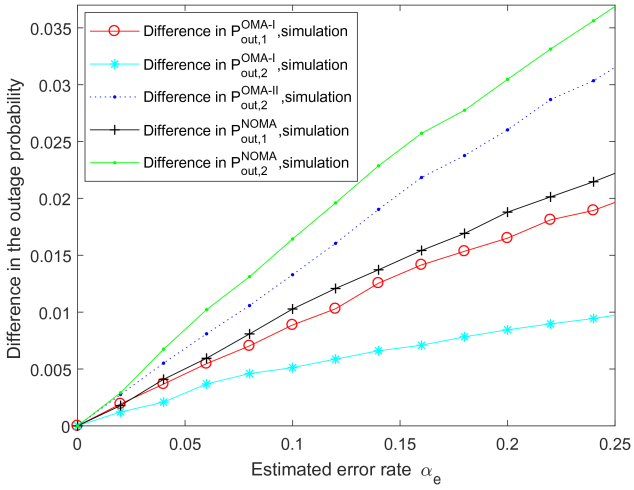

Fig. 12 *Difference between h_i and $\hat{h}_i$ in outage probability versus estimated error rate*

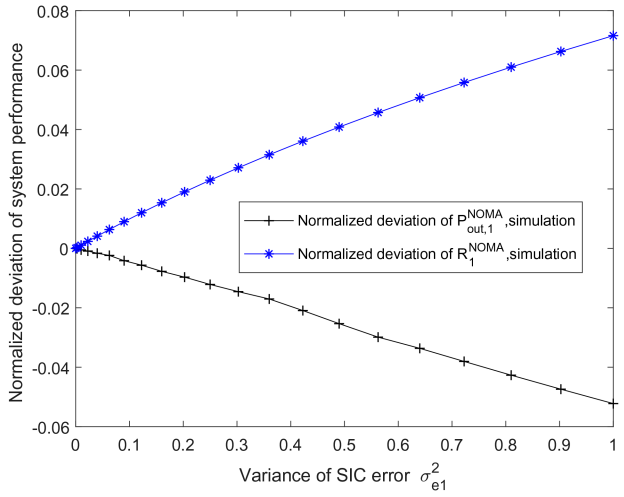

Fig. 13 *Normalised deviation of system performance versus SIC error variance*

since NOMA can transmit two user signals per slot (i.e. $x_1(n)$ and $x_2(n)$) while OMA-II only transmits one signal (i.e. $x_2(n)$). Moreover, we have found that when the SBS-SU_2 link is in bad condition, NOMA in general yields the best outage performance.

6.4 Impact of imperfect CSI and imperfect SIC

Illustrative results based on imperfect CSI estimation are presented in Fig. 12, which shows the difference between h_i and $\hat{h}_i$ in the outage probability of different schemes (e.g. $P_{\text{out},1}^{\text{NOMA}}(h_i) - P_{\text{out},1}^{\text{NOMA}}(\hat{h}_i)$) as a function of the estimated error rate (i.e. $\alpha_e = \sigma_{e,i}^2/\sigma_i^2$). It can be seen that for moderate level of error rate (e.g. $0 \le \alpha_e \le 0.25$), the outage probability is not significantly affected with increasing α_e when using the estimated channel gains instead of the true gains. Hence, it can be concluded that the results presented in this paper on the basis of exact CSI (i.e. $\alpha_e = 0$) serve as a useful theoretical bounds for application to practical situations with CSI errors.

Then, according to the case of imperfect SIC, we show the illustrative results of normalised deviation in the probability measures

$$\left(\text{i.e.}\ \frac{P_{\text{out},1}^{\text{NOMA}}(\gamma_{1,1|\nu}) - P_{\text{out},1}^{\text{NOMA}}(\gamma_{1,1|\nu}^{e})}{P_{\text{out},1}^{\text{NOMA}}(\gamma_{1,1|\nu})} \quad \text{and} \quad \frac{R_1^{\text{NOMA}}(\gamma_{1,1|\nu}) - R_1^{\text{NOMA}}(\gamma_{1,1|\nu}^{e})}{R_1^{\text{NOMA}}(\gamma_{1,1|\nu})}\right)$$

as a function of the SIC error variance in Fig. 13. It can be seen that for moderate level of error (e.g. $0 \le \sigma_{e1}^2 \le 1$), there will be a small increase in $P_{\text{out},1}^{\text{NOMA}}$ or a decrease in R_1^{NOMA} with increasing σ_{e1}^2. Hence, it can be concluded that the results achieved in this paper on the basis of perfect SIC (i.e. $\sigma_{e1}^2 = 0$) serve as a useful theoretical lower limit of $P_{\text{out},1}^{\text{NOMA}}$ and upper limit of R_1^{NOMA} for application to practical situation with SIC errors.

7 Conclusion

In this paper, we have presented a comprehensive analysis for a novel NOMA-based cooperative transmission scheme for CRN. In this scheme, the SBS first detects an unoccupied licensed channel through spectrum sensing and then transmits its data to SU_1 and SU_2 by employing the NOMA scheme and adjusting transmission parameters according to the detection results. The proposed scheme ensures that multiple users can be served simultaneously while the overall spectrum can be better utilised. The expressions of the average outage probability and ergodic sum rate for the proposed NOMA and two traditional OMA schemes have been derived and further studied by simulations. Numerical results confirmed that (i) the proposed NOMA scheme can achieve lower average outage probability than the OMA schemes, especially when the distant SU's channel is in bad condition; (ii) compared with the traditional underlay CRN transmission schemes (i.e. without spectrum sensing), determining an appropriate value of spectrum sensing time fraction (i.e. τ) is essential to improve the outage performance for the proposed system; (iii) the ergodic rate can be maximised through the optimal choice of the τ; and (iv) the ergodic sum rate of OMA-I, OMA-II and the proposed NOMA scheme is always better than the traditional underlay CRN transmission schemes. Finally, we should mention that extension of this work to the cases of imperfect CSI estimation and imperfect SIC for the multiple antennas transmission is an interesting avenue for future research, as it can lead to further improvements in spectral efficiency and bring more practical values.

8 Acknowledgments

This work was supported by the Open Research Funds of Key Lab of Broadband Wireless Communication and Sensor Network Technology, Nanjing University of Posts and Telecommunications (no. NYKL201505); the National Natural Science Foundation of China (no. 61501223).)

9 References

[1] Ding, Z., Liu, Y., Choi, J., *et al.*: 'Application of non-orthogonal multiple access in LTE and 5G networks', *IEEE Commun. Mag.*, 2017, **55**, (2), pp. 185–191

[2] Ding, Z., Lei, X., Karagiannidis, G.K., *et al.*: 'A survey on non-orthogonal multiple access for 5G networks: research challenges and future trends', *IEEE J. Sel. Areas Commun.*, 2017, **35**, (10), pp. 2181–2195

[3] Shin, W., Vaezi, M., Lee, B., *et al.*: 'Non-orthogonal multiple access in multi-cell networks: theory, performance, and practical challenges', *IEEE Commun. Mag.*, 2017, **55**, (10), pp. 176–183

[4] Qian, L.P., Wu, Y., Zhou, H., *et al.*: 'Joint uplink base station association and power control for small-cell networks with non-orthogonal multiple access', *IEEE Trans. Wirel. Commun.*, 2017, **16**, (9), pp. 5567–5582

[5] Men, J., Ge, J., Zhang, C.: 'Performance analysis of nonorthogonal multiple access for relaying networks over Nakagami-*m* fading channels', *IEEE Trans. Veh. Technol.*, 2017, **66**, (2), pp. 1200–1208

[6] Zhang, Z., Ma, Z., Xiao, M., *et al.*: 'Full-duplex device-to-device-aided cooperative nonorthogonal multiple access', *IEEE Trans. Veh. Technol.*, 2017, **66**, (5), pp. 4467–4471

[7] Zhang, L., Liu, J., Xiao, M., *et al.*: 'Performance analysis and optimization in downlink NOMA systems with cooperative full-duplex relaying', *IEEE J. Sel. Areas Commun.*, 2017, **35**, (10), pp. 2398–2412

[8] Liu, G., Chen, X., Ding, Z., *et al.*: 'Hybrid half-duplex/full-duplex cooperative non-orthogonal multiple access with transmit power adaptation', *IEEE Trans. Wirel. Commun.*, 2018, **17**, (1), pp. 506–519

[9] Zhong, C., Zhang, Z.: 'Non-orthogonal multiple access with cooperative full-duplex relaying', *IEEE Commun. Lett.*, 2016, **20**, (12), pp. 2478–2481

[10] Yue, X., Liu, Y., Kang, S., *et al.*: 'Exploiting full/half-duplex user relaying in NOMA systems', *IEEE Trans. Commun.*, 2018, **66**, (2), pp. 560–575

[11] Yuan, W., Li, P.Q., Mao, H., *et al.*: 'Optimal power allocation and scheduling for non-orthogonal multiple access relay-assisted networks', *IEEE Trans. Mob. Comput.*, 2018, **PP**, (99), pp. 1–1

[12] Akyildiz, I.F., Lee, W.Y., Vuran, M.C., *et al.*: 'A survey on spectrum management in cognitive radio networks', *IEEE Commun. Mag.*, 2008, **46**, (4), pp. 40–48

[13] Ghasemi, A., Sousa, E.S.: 'Spectrum sensing in cognitive radio networks: requirements, challenges and design trade-offs', *IEEE Commun. Mag.*, 2008, **46**, (4), pp. 32–39

[14] Wang, B., Liu, K.J.R.: 'Advances in cognitive radio networks: a survey', *IEEE J. Sel. Top. Sign. Proces.*, 2011, **5**, (1), pp. 5–23

[15] Ganesan, G., Li, Y.: 'Cooperative spectrum sensing in cognitive radio, part I: two user networks', *IEEE Trans. Wirel. Commun.*, 2007, **6**, (6), pp. 2204–2213

[16] Ganesan, G., Li, Y.: 'Cooperative spectrum sensing in cognitive radio, part II: multiuser networks', *IEEE Trans. Wirel. Commun.*, 2007, **6**, (6), pp. 2214–2222

[17] Hecke, J.V., Fiorentino, P.D., Lottici, V., *et al.*: 'Distributed dynamic resource allocation for cooperative cognitive radio networks with multi-antenna relay selection', *IEEE Trans. Wirel. Commun.*, 2017, **16**, (2), pp. 1236–1249

[18] Elmahdy, A.M., El-Keyi, A., ElBatt, T., *et al.*: 'Optimizing cooperative cognitive radio networks performance with primary QoS provisioning', *IEEE Trans. Commun.*, 2017, **65**, (4), pp. 1451–1463

[19] Zhang, L., Xiao, M., Wu, G., *et al.*: 'A survey of advanced techniques for spectrum sharing in 5G networks', *IEEE Wirel. Commun.*, 2017, **24**, (5), pp. 44–51

[20] Zhou, F., Wu, Y., Liang, Y., *et al.*: 'State of the art, taxonomy, and open issues on cognitive radio networks with NOMA', *IEEE Wirel. Commun.*, 2018, **25**, (2), pp. 100–108

[21] Liu, Y., Ding, Z., Elkashlan, M., *et al.*: 'Nonorthogonal multiple access in large-scale underlay cognitive radio networks', *IEEE Trans. Veh. Technol.*, 2016, **65**, (12), pp. 10152–10157

[22] Lv, L., Chen, J., Ni, Q.: 'Cooperative non-orthogonal multiple access in cognitive radio', *IEEE Commun. Lett.*, 2016, **20**, (10), pp. 2059–2062

[23] Lv, L., Chen, J., Ni, Q., *et al.*: 'Design of cooperative non-orthogonal multicast cognitive multiple access for 5G systems: user scheduling and performance analysis', *IEEE Trans. Commun.*, 2017, **65**, (6), pp. 2641–2656

[24] Lv, L., Ni, Q., Ding, Z., *et al.*: 'Application of non-orthogonal multiple access in cooperative spectrum-sharing networks over Nakagami- m fading channels', *IEEE Trans. Veh. Technol.*, 2017, **66**, (6), pp. 5506–5511

[25] Lee, S., Duong, T.Q., daCosta, D.B., *et al.*: 'Underlay cognitive radio networks with cooperative non-orthogonal multiple access', *IET Commun.*, 2018, **12**, pp. 359–366(7)

[26] Mohammadi, M., Chalise, B.K., Hakimi, A., *et al.*: 'Beamforming design and power allocation for full-duplex non-orthogonal multiple access cognitive relaying', *IEEE Trans. Commun.*, 2018, **66**, pp. 1–1

[27] Lu, L., Jian, C., Qiang, N., *et al.*: 'Cognitive non-orthogonal multiple access with cooperative relaying: A new wireless frontier for 5G spectrum sharing', *IEEE Commun. Mag.*, 2018, **PP**, (99), pp. 1–8

[28] Zou, Y., Yao, Y.D., Zheng, B.: 'Outage probability analysis of cognitive transmissions: impact of spectrum sensing overhead', *IEEE Trans. Wirel. Commun.*, 2010, **9**, (8), pp. 2676–2688

[29] Zhang, H., Nie, Y., Cheng, J., *et al.*: 'Sensing time optimization and power control for energy efficient cognitive small cell with imperfect hybrid spectrum sensing', *IEEE Trans. Wirel. Commun.*, 2017, **16**, (2), pp. 730–743

[30] Liang, Y.C., Zeng, Y., Peh, E.C.Y., *et al.*: 'Sensing-throughput tradeoff for cognitive radio networks', *IEEE Trans. Wirel. Commun.*, 2008, **7**, (4), pp. 1326–1337

[31] Khan, A.A., Rehmani, M.H., Reisslein, M.: 'Cognitive radio for smart grids: survey of architectures, spectrum sensing mechanisms, and networking protocols', *Commun. Surveys Tuts.*, 2016, **18**, (1), pp. 860–898

[32] Kusaladharma, S., Herath, P., Tellambura, C.: 'An overview of cognitive radio networks', in Kusaladharma, S., Herath, P., Tellambura, C. (Eds.): '*An overview of cognitive radio networks, Wiley encyclopedia of electrical and electronics engineering*' (Wiley, Hoboken, NJ, USA, 2017)

[33] Zou, Y., Zheng, B., Zhu, J.: 'Outage analysis of opportunistic cooperation over rayleigh fading channels', *IEEE Trans. Wirel. Commun.*, 2009, **8**, (6), pp. 3077–3085

[34] Abramowitz, M., Stegun, I. (Eds.): '*Handbook of mathematical functions with formulas, graphs, and mathematical tables*' (Dover Publications Inc.,, New York, 1972)

[35] Jeffrey, A., Zwillinger, D. (Eds.): '*Table of integrals, series, and products*' (Academic Press, Burlington, USA, 2007, 7th edn.

[36] Fang, F., Zhang, H., Cheng, J., *et al.*: 'Joint user scheduling and power allocation optimization for energy-efficient noma systems with imperfect CSI', *IEEE J. Sel. Areas Commun.*, 2017, **35**, (12), pp. 2874–2885

[37] Chen, X., Jia, R., Ng, D.W.K.: 'On the design of massive non-orthogonal multiple access with imperfect successive interference cancellation', *IEEE Commun.*, 2019, **67**, (3), pp. 2539–2551

[38] Li, S., Derakhshani, M., Lambotharan, S.: 'Outage-constrained robust power allocation for downlink mc-noma with imperfect sic'. 2018 IEEE Int. Conf. on Communications (ICC), Kansas City, USA, 2018, pp. 1–7

10 Appendix

10.1 Proof of Proposition 1

By introducing $\mathcal{O}_{11} = \Pr(|h_{s1}|^2 < (\omega/(\rho_{s|\nu})))$, $\mathcal{O}_{12} = \Pr(|h_{s2}|^2 < (\omega/(\rho_{s|\nu})))$, $\mathcal{O}_{21} = 1 - \mathcal{O}_{11}$ and

$$\mathcal{O}_{22} = \Pr\Big(\frac{\alpha_2 |h_{s2}|^2}{\alpha_1 |h_{s2}|^2 + \frac{1}{\rho_{s|\nu}}} + |h_{12}|^2 \rho_{r|\nu} < u_2\Big),$$

and using (13) and (15), $\Pr(\Theta_1')$ in (39) can be rewritten as

$$\Pr(\Theta_1') = \sum_{\nu=0}^{1} \Pr(\widehat{H}_\nu)\mathcal{O}_{11}\mathcal{O}_{12}, \tag{58}$$

then, based on (13) and (21), $\Pr(\Theta_2')$ in (40) can be rewritten as

$$\Pr(\Theta_2') = \sum_{\nu=0}^{1} \Pr(\widehat{H}_\nu)\mathcal{O}_{21}\mathcal{O}_{22}. \tag{59}$$

The various probabilities $\mathcal{O}_{ij}$ in the preceding equations can be expressed as

$$\mathcal{O}_{11} = \begin{cases} 1, & u_2 \geq \dfrac{\alpha_2}{\alpha_1}, \\ 1 - \exp\Big(-\dfrac{\omega}{\lambda_1}\Big), & u_2 < \dfrac{\alpha_2}{\alpha_1}, \end{cases} \tag{60}$$

$$\mathcal{O}_{12} = \begin{cases} 0, & u_2 \geq \dfrac{\alpha_2}{\alpha_1}, \\ \exp\Big(-\dfrac{\omega}{\lambda_2}\Big), & u_2 < \dfrac{\alpha_2}{\alpha_1}. \end{cases} \tag{61}$$

By substituting (60) and (61) into (39), a closed-form expression for $\Pr(\Theta_2')$ is obtained as given in (41).

Next, with the help of (60), we can get $\Pr(\Theta_2') = 0$ when $u_2 \geq \alpha_2/\alpha_1$. Then, we are left with the case $u_2 < \alpha_2/\alpha_1$. By denoting

$$\Phi = \frac{\alpha_2 |h_{s2}|^2}{\alpha_1 |h_{s2}|^2 + \frac{1}{\rho_{s|\nu}}},$$

$\mathcal{O}_{22}$ can be calculated as

$$\begin{aligned} \mathcal{O}_{22} &= \int_0^{u_2} \Pr\Big(|h_{12}|^2 < \frac{u_2 - \varphi}{\rho_{r|\nu}}\Big) f_\Phi(\varphi)\,\mathrm{d}\varphi \\ &= F_\Phi(u_2) - \frac{u_2}{2}\exp\Big(-\frac{u_2}{\lambda_3}\Big)\int_{-1}^{1} \exp\Big(\frac{\varphi_1}{\lambda_3}\Big) f_\Phi(\varphi_1)\,\mathrm{d}x, \end{aligned} \tag{62}$$

where $\varphi_1 = (u_2 x + u_2)/2$. Making use of the Gaussian–Chebyshev quadrature [34, eq.(25.4.38)], (62) can be approximated by

$$\begin{aligned} \mathcal{O}_{22} \simeq F_\Phi(u_2) &- \frac{u_2\pi}{2(n+1)}\exp\Big(-\frac{u_2}{\lambda_3}\Big) \\ &\cdot \sum_{k=0}^{K} \sqrt{(1 - x_k^2)}\exp\Big(\frac{y_k}{\lambda_3}\Big) f_\Phi(y_k), \end{aligned} \tag{63}$$

where K is the Gaussian-Chebyshev parameter controlling the complexity-accuracy tradeoff, $x_k = \cos(((2k+1)\pi)/(2(K+1)))$, $y_k = (u_2/2)(x_k + 1)$, while $F_\Phi(u_2) = 1 - \exp(-(\omega/\lambda_2))$ and

$$f_\Phi(\varphi) = \frac{\alpha_2}{\lambda_2(\alpha_2 - \alpha_1\varphi)^2}\exp\Big(-\frac{\varphi}{\lambda_2(\alpha_2 - \alpha_1\varphi)}\Big).$$

By substituting (63) into (59), an approximate closed-expression for $\Pr(\Theta_2')$ is obtained as given in (42).